symmetry

IMPACT FACTOR 2.2

CITESCORE 5.4

Article

Stable Majorana Zero-Energy Modes in Two-Dimensional Josephson Junctions

Yuting Huang, Qinyi Wang, Lei Li and Zhenying Wen

MDPI

https://doi.org/10.3390/sym16081066

symmetry

MDPI

Article

Stable Majorana Zero-Energy Modes in Two-Dimensional Josephson Junctions

Yuting Huang [1], Qinyi Wang [1], Lei Li [1,2] and Zhenying Wen [1,*]

[1] Center for Theoretical Physics, College of Physics, Sichuan University, Chengdu 610065, China; huangyuting1@stu.scu.edu.cn (Y.H.)
[2] College of Physics and Electronic Information, Sichuan University of Science and Engineering, Yibin 643000, China
* Correspondence: wenzy@scu.edu.cn

Abstract: In this paper, a modified Josephson junction model is proposed, which splits the two-dimensional electron gas by inserting a middle superconductor strip into a conventional Josephson junction. This modification enhances the superconducting proximity effect, thus avoiding the appearance of a soft gap and inducing a stable Majorana zero-energy mode. Through numerical simulation, the impact of the middle superconductor strip with different widths on the energy band structure is studied, and a significant increase in the topological energy gap is found. In addition, the modified system maintains a robust topological gap even at a strong in-plane magnetic field.

Keywords: Majorana zero-energy mode; Josephson junction; band structures; symmetry breaking

1. Introduction

The Majorana zero-energy modes (MZMs), as quasiparticles, exhibit non-Abelian anyonic statistics in condensed matter physics [1–4]. MZMs exhibit non-Abelian statistics, meaning that when the positions of two MZMs are exchanged, the systems will usually end in different states from the original one. It has been predicted in topologically non-trivial quantum matters such as the boundaries of one-dimensional topological superconductors and the vortex cores of two-dimensional topological superconductors [5–7]. The research of MZMs is not only significant for fundamental physics but also holds promising applications in realizing topological quantum computation. Due to their robustness of local perturbations, MZMs become good candidates for realizing fault-tolerant quantum computation [8,9]. Furthermore, the non-Abelian exchange statistics of MZMs also provides new possibilities for quantum information coding, which may lead to a significant improvement in the power and security of quantum computers [10].

Topological superconductivity is a special superconducting state [11], which has non-trivial topological properties and also has the zero resistance and complete diamagnetism of superconductors. These properties are mainly manifested in the existence of stable zero-energy modes at the edge or defect of materials. The existence of superconducting gaps in the band structures of topological superconductors is related to the properties of the system. The existence of a topological gap is also a necessary condition for the emergence and stability of MZMs [12,13]. The topological superconductor platform is a promising candidate for the realization of MZMs. It can be divided into intrinsic topological superconductors and artificial topological superconductors [14]. Most current experiments focus on one-dimensional semiconducting nanowires with specific materials [15]. A hybrid system based on s-wave superconductors and topological insulators was proposed by Fu and Kane [16]. This scheme uses the superconducting proximity effects and the spin–orbit coupling on the surface of topological insulators to recreate Kitaev's one-dimensional chain model. After that, Lutchyn and Oreg independently extended this assumption to

check for updates

Citation: Huang, Y.; Wang, Q.; Li, L.; Wen, Z. Stable Majorana Zero-Energy Modes in Two-Dimensional Josephson Junctions. *Symmetry* **2024**, *16*, 1066. https://doi.org/10.3390/sym16081066

Academic Editor: Sergio Caprara

Received: 2 July 2024
Revised: 13 August 2024
Accepted: 16 August 2024
Published: 19 August 2024

the semiconductor–superconductor heterostructures [8,17–19] which belong to artificial topological superconductors.

Another important heterostructure system is the two-dimensional Josephson junction proposed in 2017 [20,21]. They proposed a setup that could couple multiple MZMs to achieve the braiding operations required for topological quantum computing. Pientka calculated the local density of states (LDOS) around the boundary of the systems based on the tight-binding model of the Hamiltonian, thus verifying the appearance of MZMs in the system, with the position of the MZMs being confined to both ends of the Josephson junction. This kind of setup can also be combined with other Josephson junction systems to achieve extensible quantum bit design [22,23]. The two-dimensional hybrid system introduces superconducting phase difference control methods [20,21,24,25] and retains gate voltage control methods [10], allowing for more precise control of the positions and quantities of MZMs compared to the one-dimensional full-shell nanowire system. Recently, a similar scheme based on a superconductor–normal–superconductor (SNS) hybrid system was proposed [26], which is expected to greatly reduce the required magnetic field in addition to the advantages above [27]. Therefore, seeking a way to create stable MZMs based on this kind of SNS hybrid system becomes the focus of our work.

Introducing the superconducting phase difference control method in the two-dimensional SNS Josephson junction can effectively reduce the critical magnetic field B_{crit} which is required to induce the topological phase. When the phase difference between the two superconductors reaches $\phi = \pi$, the topological phase transition can be achieved at a lower external magnetic field [20], and the destruction of the topological gap can be avoided. Meanwhile, the superconducting phase difference generated by supercurrent or gate electrodes also allows us to control and modify MZMs by electrical means [21,22] so that it has a broad application prospect.

Recent experiments have realized some two-dimensional hybrid SNS systems based on superconducting phase difference, where topological non-trivial phases predicted by the theory are successfully observed through zero-bias conductance peaks [28–30] or directly measuring the phase [31–33]. However, due to the influence of quasiparticle trajectories in the two-dimensional electron gas region [34], soft gaps that impact the stability of MZMs still appeared in the experiments [35]. In order to eliminate the soft gap that appeared in these experiments, many studies have attempted to find out the cause of the soft gap in MZMs induced by the superconducting phase difference [36]. From a semiclassical point of view, $E_{\text{gap}} \simeq \hbar v_F / L_t$ when the width of the semiconductor W is much smaller than the trajectory L_t, based on Thouless's theory. Thus, a long electron's trajectory induced by momentum along the direction of translation symmetry in a straight junction reduces the E_{gap}. One can tackle this problem by designing a new experimental setup with a serrated normal region to shorten trajectories by geometric constraints [37,38].

In this work, we propose a new setup of SNS Josephson junctions to create stable Majorana zero modes based on the superconducting phase difference and external magnetic field. We insert a third superconductor layer in a Josephson junction to form a modified system, in which the Andreev energy levels are not degenerate anymore, so time-reversal symmetry breaking can be achieved in this system [39–42]. Moreover, this modified setup can be realized and modulated in experiments. Our work mainly focuses on analyzing the band structures of the new system and finding the optimal conditions for generating stable MZMs.

2. Setup

The Josephson junction consists of a 2D strip of a semiconductor and two superconductors on both sides [20,21]. One can modify the original junction by inserting a thin superconducting strip in the middle of the semiconductor strip. This modified system can create the hard-induced superconducting gap and eliminate the impact of the soft gap. We set the x-axis parallel to the Josephson junction and the y-axis perpendicular to the Josephson junction as shown in Figure 1.

The two-dimensional electron gas (2DEG) with a x-direction magnetic field is the blue region, and its Hamiltonian reads [43]

$$\hat{H}_{\mathrm{N}} = \left[\frac{\hat{p}_x^2 + \hat{p}_y^2}{2m_{\mathrm{eff}}} - \mu\right]\sigma_0\tau_z + \alpha(\hat{p}_y\sigma_x - \hat{p}_x\sigma_y)\tau_z + \frac{1}{2}g\mu_B B_x\sigma_x\tau_0. \quad (1)$$

The yellow regions are the superconductors with different superconducting phases, and the Hamiltonian is

$$\hat{H}_{\mathrm{S}} = \left[\frac{\hat{p}_x^2 + \hat{p}_y^2}{2m_{\mathrm{eff}}} - \mu\right]\sigma_0\tau_z + \Delta\cos\varphi\sigma_0\tau_x + \Delta\sin\varphi\sigma_0\tau_y. \quad (2)$$

Here, $\hat{p}_x$ and $\hat{p}_y$ are the momenta of the electrons. For the 2DEG material, m_{eff} is the effective electron mass, μ is the chemical potential, α is the spin–orbit coupling strength, and g is the Landé g factor, so the $\frac{1}{2}g\mu_B B_x$ denotes the Zeeman splitting in the x-direction [44]. For the s-wave superconductor, Δ represents the coupling strength of the s-wave superconductors, and Δ' is the coupling strength of the middle superconductor. The superconducting phase difference between the top and bottom superconductors is $\phi = \pi$, so the superconducting phases of these two superconductors are $\varphi = \pm\frac{\phi}{2} = \pm\frac{\pi}{2}$, and the superconducting phases of the middle superconductor is $\varphi' = 0$.

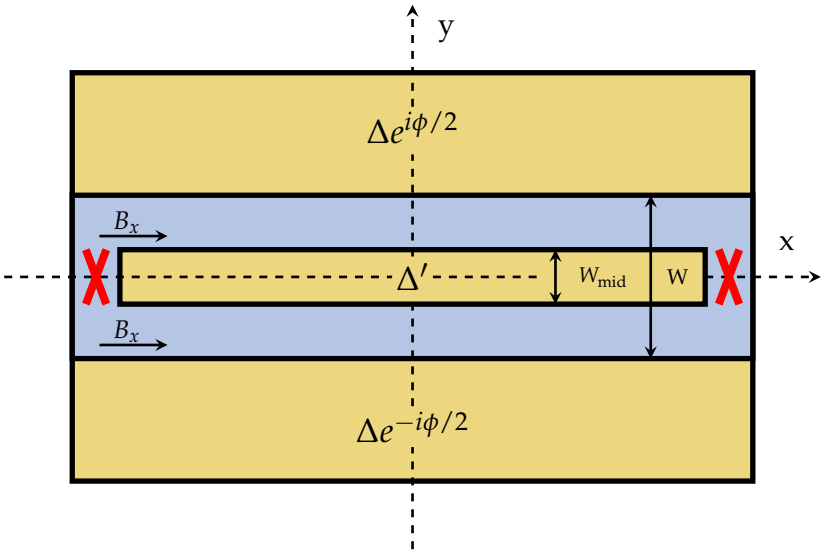

Figure 1. The modified Josephson junction. The distance between the two superconductors remains $W = 200$ nm, unchanged, and the width of the middle superconducting layer W_{mid} varies.

Therefore, for the three different s-wave superconductors with different coupling strengths Δ and superconducting phases φ, we can distinguish the Hamiltonian in these three regions. The Hamiltonian of the top and bottom superconductors is

$$\hat{H}_{\mathrm{T,B}} = \left[\frac{\hat{p}_x^2 + \hat{p}_y^2}{2m_{\mathrm{eff}}} - \mu\right]\sigma_0\tau_z + \Delta\cos(\pm\frac{\pi}{2})\sigma_0\tau_x + \Delta\sin(\pm\frac{\pi}{2})\sigma_0\tau_y. \quad (3)$$

The Hamiltonian of the middle superconductor where $\varphi' = 0$ reads

$$\hat{H}_{\mathrm{M}} = \left[\frac{\hat{p}_x^2 + \hat{p}_y^2}{2m_{\mathrm{eff}}} - \mu\right]\sigma_0\tau_z + \Delta'\cos(0)\sigma_0\tau_x + \Delta'\sin(0)\sigma_0\tau_y. \quad (4)$$

The middle superconductor is not essentially different from the original two superconductors, so we can take $\Delta' = \Delta$.

In this two-dimensional system, the Hamiltonian acts on the Nambu basis $\Psi(x,y) = (\Psi_{e\uparrow}, \Psi_{e\downarrow}, \Psi_{h\downarrow}, -\Psi_{h\uparrow})^T$, and the Pauli matrices σ_i act on spin degrees of freedom $\Psi_\uparrow$ or $\Psi_\downarrow$ and τ_i act on particle degrees of freedom Ψ_e or Ψ_h. Hence, we can analyze the system's symmetry on the Nambu basis.

3. Symmetry

Based on the modified setup, we can obtains the expression of its Hamiltonian, which can be used to analyze the symmetries

$$\hat{H} = \begin{cases} [\frac{\hat{p}_x^2+\hat{p}_y^2}{2m_{\text{eff}}} - \mu]\sigma_0\tau_z + \Delta'\sigma_0\tau_x & |y| < W_{\text{mid}}/2 \\ [\frac{\hat{p}_x^2+\hat{p}_y^2}{2m_{\text{eff}}} - \mu]\sigma_0\tau_z + \alpha(\hat{p}_y\sigma_x - \hat{p}_x\sigma_y)\tau_z + \frac{1}{2}g\mu_B B_x\sigma_x\tau_0 & W_{\text{mid}}/2 < |y| < W/2 \\ [\frac{\hat{p}_x^2+\hat{p}_y^2}{2m_{\text{eff}}} - \mu]\sigma_0\tau_z \pm \Delta\sigma_0\tau_y & W/2 < |y| \end{cases} \quad (5)$$

Similar to the experimental junction [24,28], the spatial symmetry of our system can be analyzed directly based on this Hamiltonian and Figure 1. For the $y > 0$ region, under the spatial inversion transform $y \to -y$,

$$+\phi/2 \to -\phi/2, \qquad \hat{p}_y \to -\hat{p}_y. \quad (6)$$

The transformed expression for its Hamiltonian corresponds to the $y < 0$ region, and vice versa.

The time-reversal operator for the spin-1/2 system is

$$\mathcal{T} = -i\sigma_y\mathcal{K}, \quad (7)$$

where $\mathcal{K}$ is the complex conjugate operator [45]. The Hamiltonian for different regions under the time-reversal transformation is as follows. For the 2EDG region, the Hamiltonian $\hat{H}_N$ transforms as

$$\mathcal{T}\hat{H}_N(\hat{\mathbf{r}},\hat{\mathbf{p}})\mathcal{T}^{-1} = [\frac{\hat{p}_x^2+\hat{p}_y^2}{2m_{\text{eff}}} - \mu]\sigma_0\tau_z + \alpha[\hat{p}_y\sigma_x - \hat{p}_x\sigma_y]\tau_z. \quad (8)$$

And the Hamiltonian $\hat{H}_S$ for s-wave superconductors with different superconducting phases can be shown as

$$\mathcal{T}\hat{H}_S(\hat{\mathbf{r}},\hat{\mathbf{p}})\mathcal{T}^{-1} = [\frac{\hat{p}_x^2+\hat{p}_y^2}{2m_{\text{eff}}} - \mu]\sigma_0\tau_z + \Delta\cos\varphi\sigma_0\tau_x + \Delta\sin\varphi\sigma_0(-\tau_y). \quad (9)$$

The Hamiltonian $\hat{H}_M$ for the middle superconductor with $\varphi = 0$ is time-reversal symmetrical, which can be shown as

$$\mathcal{T}\hat{H}_M(\hat{\mathbf{r}},\hat{\mathbf{p}})\mathcal{T}^{-1} = [\frac{\hat{p}_x^2+\hat{p}_y^2}{2m_{\text{eff}}} - \mu]\sigma_0\tau_z + \Delta\sigma_0\tau_x. \quad (10)$$

Similarly, when the superconducting phases $\pm\phi/2 = 0$, both the top and the bottom superconductors $\hat{H}_{T,B}$ have time-reversal symmetry,

$$\mathcal{T}\hat{H}_{T,B}(\hat{\mathbf{r}},\hat{\mathbf{p}})\mathcal{T}^{-1} = \hat{H}_{T,B}(\hat{\mathbf{r}},\hat{\mathbf{p}}). \quad (11)$$

But when introducing the superconducting phase difference $\phi = \pi$, the Hamiltonian $\hat{H}_{T,B}$ with superconducting phases $\varphi = \pm\frac{\pi}{2}$ do not keep the time-reversal symmetry

$$\mathcal{T}\hat{H}_{T,B}(\hat{\boldsymbol{r}},\hat{\boldsymbol{p}})\mathcal{T}^{-1} = \big[\frac{\hat{p}_x^2+\hat{p}_y^2}{2m_{\text{eff}}} - \mu\big]\sigma_0\tau_z \pm \Delta\sigma_0(-\tau_y). \tag{12}$$

whereas for the 2DEG region, the time-reversal symmetry can be broken by an applied in-plane magnetic field B_x,

$$\mathcal{T}\hat{H}_N(\hat{\boldsymbol{r}},\hat{\boldsymbol{p}})\mathcal{T}^{-1} = \big[\frac{\hat{p}_x^2+\hat{p}_y^2}{2m_{\text{eff}}} - \mu\big]\sigma_0\tau_z + \alpha\big[\hat{p}_y\sigma_x - \hat{p}_x\sigma_y\big]\tau_z - \frac{1}{2}g\mu_B B_x\sigma_x\tau_0. \tag{13}$$

We can also define the particle–hole operator

$$\mathcal{P} = i\tau_y\mathcal{T} = \tau_y\sigma_y\mathcal{K}, \tag{14}$$

which anti-commutes with the Hamiltonian $\hat{H}$ with particle–hole symmetry as $[\mathcal{P},\hat{H}]_+ = 0$. Therefore, under the action of the particle–hole symmetry, the Hamiltonians in different regions transform as

$$\mathcal{P}\hat{H}_N(\hat{\boldsymbol{r}},\hat{\boldsymbol{p}})\mathcal{P}^{-1} = -\big[\frac{\hat{p}_x^2+\hat{p}_y^2}{2m_{\text{eff}}} - \mu\big]\sigma_0\tau_z - \alpha\big[\hat{p}_y\sigma_x - \hat{p}_x\sigma_y\big]\tau_z - \frac{1}{2}g\mu_B B_x\sigma_x\tau_0, \tag{15}$$

and for the s-wave superconductor regions, the Hamiltonian $\hat{H}_S$

$$\mathcal{P}\hat{H}_S(\hat{\boldsymbol{r}},\hat{\boldsymbol{p}})\mathcal{P}^{-1} = -\big[\frac{\hat{p}_x^2+\hat{p}_y^2}{2m_{\text{eff}}} - \mu\big]\sigma_0\tau_z - \Delta\cos\varphi\sigma_0\tau_x - \Delta\sin\varphi\sigma_0\tau_y. \tag{16}$$

As a result, the Hamiltonians in different regions are protected by particle–hole symmetry for the arbitrary in-plane magnetic field B_x and superconducting phase difference as

$$\mathcal{P}\hat{H}(\hat{\boldsymbol{r}},\hat{\boldsymbol{p}})\mathcal{P}^{-1} = -\hat{H}(\hat{\boldsymbol{r}},\hat{\boldsymbol{p}}). \tag{17}$$

Our system has both particle–hole symmetry and time-reversal symmetry. It is in the symmetry class BDI with the $\mathbb{Z}$ topological invariant without the in-plane magnetic fields. When the time-reversal symmetry is broken, the system reduces into symmetry class D, with the $\mathbb{Z}_2$ topological invariant, which depends on the parity of the $\mathbb{Z}$ topological invariant [46,47]. Therefore, the topological phase transition will occur when the $\mathbb{Z}$ topological invariant changes from even to odd, and MZMs arise in the non-trivial topological phase at the boundary of the system [20,21].

However, based on the above analysis, the introduction of the new superconducting layer with $\varphi' = 0$ does not break the time-reversal symmetry of this system, so the magnetic fields which can break the time-reversal symmetry and induce topological phase transitions are still necessary to create MZMs.

4. Band Structures

To describe the behavior of the system's band structures under different conditions, we apply the finite difference approximation to the continuum Hamiltonian. We follow the similar steps of Melo [48] and implement the tight-binding model by using the Kwant software package [49] (1.4.3) to discretize the above continuous Hamiltonian onto a square grid with lattice constant $a = 10$ nm[50].

Based on the translation symmetry in the x direction of the system, we can calculate the band structures at different momenta by applying the sparse diagonalization method to the tight-binding Hamiltonian [10]. Except for the magnetic field B_x and the width of the middle superconducting layer W_{mid}, in this article, all other system parameters are set

to the following values: $m_{\text{eff}} = 0.04m_e$; $g = 13$; $\mu = 0.2$ meV; $\alpha = 10$ meV nm; $\Delta = 1$ meV; $W = 200$ nm; and $L_{SC} = 400$ nm.

Consider a Josephson junction without a middle superconductor layer ($W = 200$ nm and $W_{\text{mid}} = 0$) and create a superconducting phase difference $\phi = \pi$ in the superconductors at both ends. The band structures of this junction are shown in Figure 2. The red dashed line represents the case where the external magnetic field $B_x = 0$, and the band structures cross, indicating that the proximity effect of superconductivity is weak when the width of the Josephson junction $W = 200$ nm. The solid line represents the band structures of the Josephson junction with an external magnetic field $B_x = 0.5$T, and it does not cross, so the system has a topological gap. Introducing a superconducting phase difference allows the system to induce topological phase transitions and generate the MZMs at lower external magnetic fields.

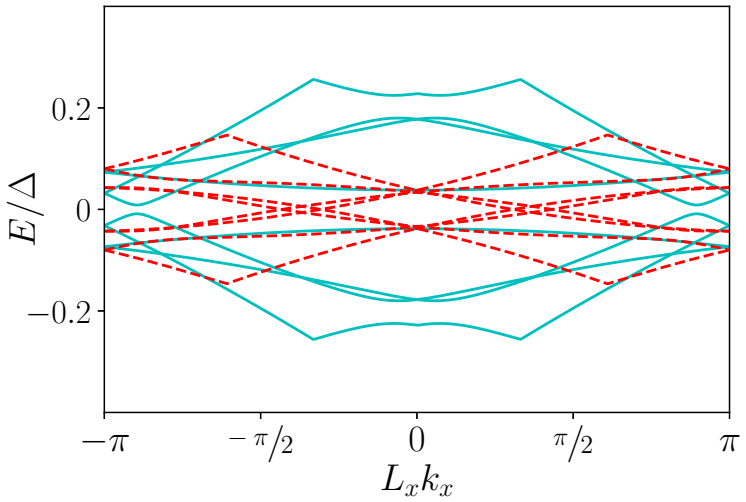

Figure 2. Band structures of the Josephson junction in the case of $W_{\text{mid}} = 0$ and $\phi = \pi$. The dashed line represents the normal state without an external magnetic field, and the solid line represents the topological state with an external magnetic field $B_x = 0.5$T. There are mini gaps at some specific k_x in the band structures of MZMs induced by the external magnetic field.

However, as in the results of the previous experiments, the topological gap induced by the magnetic field is soft and unstable. To this end, we insert a superconducting strip inside the two-dimensional electron gas to enlarge the topological gap of the system.

5. Results and Discussion

We establish a modified Josephson junction by inserting a middle superconductor strip inside the semiconductor. The width of the modified Josephson junction is $W = 200$ nm. The numerical simulation results of the modified setup are shown in Figure 3, which can demonstrate the effect of different widths of the new superconductor layer W_{mid} on this system.

Our modified system significantly changes the width of the 2DEG region of the Josephson junction by inserting the width of the intermediate superconducting layer because the width of the 2DEG electron gas region affects the ease with which the system enters the topological superconducting phase. In most cases, decreasing the width of the 2DEG region leads to stronger superconducting proximity effects, allowing the system to be induced into the topological phase by lower magnetic fields (or even zero magnetic fields). The superconducting phase difference of the superconductors at both ends can induce the system to have a certain topological gap, and the width of the 2DEG region affects the size and distribution of this induced topological gap [51], thus affecting the formation and observation of MZMs. On the contrary, increasing the width of the 2deg region decreases the induced topological gap, making the system require a stronger magnetic field to obtain

the topological phase transition. However, the 2DEG region width also affects the degree of MZMs localization at the edges, and a larger 2DEG region width makes the MZMZs more localized and thus easier to detect and manipulate.

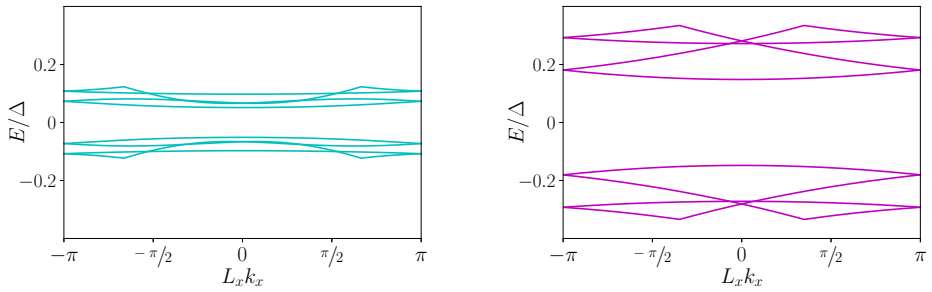

(**a**) $W_{mid} = 30$ nm (**b**) $W_{mid} = 90$ nm

Figure 3. Band structures of Josephson junction with third superconductor layer in the case of an external magnetic field $B_x = 0.5$T.

To study the effects of different widths of the middle superconductor strip on the topological gap as well as on the stability of the MZMs, we calculate the band structures of the modified Josephson junction with two different superconductor strip widths $W_{\text{mid}} = 30$ nm and $W_{\text{mid}} = 30$ nm. Compared with the Josephson junction without the middle superconductor strip indicated by the blue solid line in Figure 1, the 2DEG region of the modified Josephson junction with the insertion of the middle superconductor will be decomposed into two smaller regions as shown in Figure 2. Moreover, since we fix the total width of the Josephson junction at $W = 200$ nm, compared with the case where the middle superconductor strip width $W_{\text{mid}} = 30$ nm, when $W_{\text{mid}} = 90$ nm, the 2DEG region of the modified Josephson junction will be shrunk, so the superconducting proximity effects in the junction will be enhanced. Therefore, the topological gap will increase with the increase in the strip's width, and the band structures of the Josephson junction will flatten after inserting the middle superconductor strip.

The in-plane magnetic field is the main way to induce and regulate the topological phase transition, and the magnetic field that affects the realization of the MZMs is mainly parallel to the 2DEG region. The magnetic field in this direction plays a key role in realizing the topological superconducting phase and observing the Majorana zero mode. In the Josephson junction, the external magnetic field induces a topological phase transition of the system from the trivial phase to the topological superconducting phase, which is crucial for creating and observing MZMs. When the magnetic field is sufficiently large compared to the superconducting energy gap, a zero-bias conductance peak can be observed, which is an important indication of the presence of MZMs.

To verify the stability of the Majorana zero-energy mode and search for the most suitable experimental conditions, we conduct band structure simulations under various in-plane magnetic fields in Figure 4. The results in Figure 4a show that when the in-plane magnetic field $B_x = 0$, there is no band crossing in the system, indicating the presence of a tough gap. However, since the time-reversal symmetry is not broken, the system remains in a trivial topological phase without MZMs. When the in-plane magnetic field of the system is at a lower value such as $B_x = 0.25$T or $B_x = 0.5$T, the time-reversal symmetry of the system is broken by the magnetic field. It allows the system to enter the topological non-trivial phase more easily. In Figure 4b,c, we calculate the band structures of the system at $B_x = 0.25$T or $B_x = 0.5$T. A wide topological energy gap can be observed in both figures, indicating that the system's band structures have a stable hard induced energy gap under a lower in-plane magnetic field. So it also means that this is an ideal condition for creating stable MZMs. We also calculate the band structure at $B_x = 1$T (Figure 4d). Even with a strong magnetic field, the system band structures still have no band crossing.

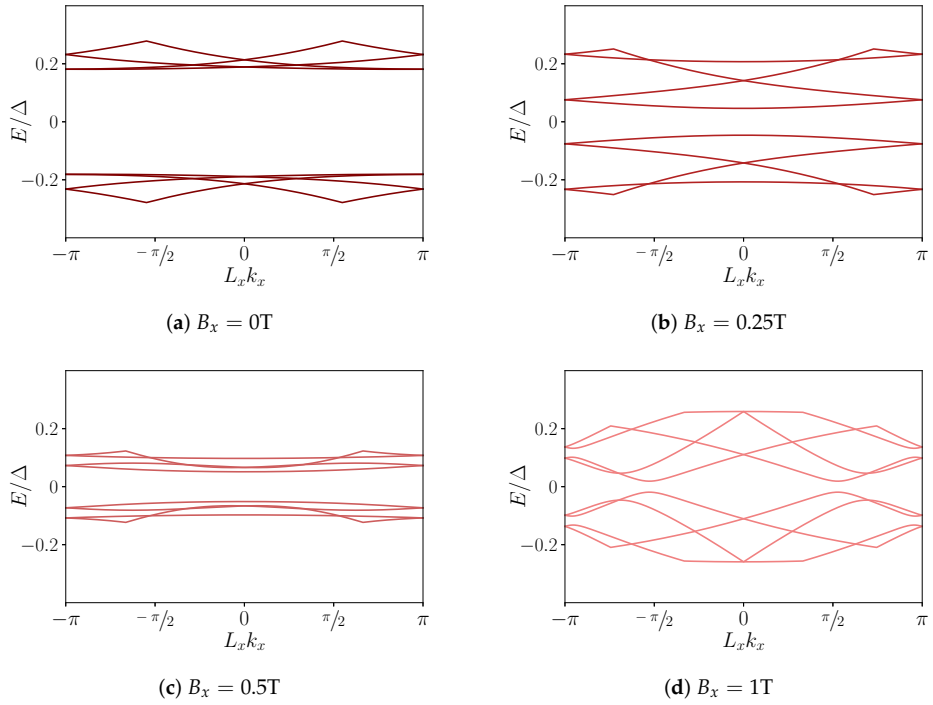

(**a**) $B_x = 0$T (**b**) $B_x = 0.25$T

(**c**) $B_x = 0.5$T (**d**) $B_x = 1$T

Figure 4. Band structures of Josephson junction with the width of the middle superconductor layer $W_{\text{mid}} = 30$ nm and different external magnetic fields.

Therefore, based on our results, we find that the topological gap of the band structures will gradually decrease as the in-plane magnetic field increases. In particular, when the magnetic field is $B_x = 1$T, severe damage to the topological gap is observed in the previous experimental platform, which is not conducive to generating stable MZMs. However, the result in Figure 4d shows that the modified system still has a topological gap at $B_x = 1$T. It implies that our modified system can generate MZMs in a wider range of magnetic field conditions.

In the Josephson junction, precision devices such as superconducting quantum interferometry devices are used to precisely control the magnetic flux through the Josephson junction. Especially in small superconducting junctions, the in-plane magnetic field can change the energy-gap structures of the system, leading to the closure and opening of the topological gap, which are important implications for the observation and manipulation of MZMs. In conclusion, the magnetic field is a key factor in creating and controlling MZMs in 2D superconducting systems, and the physical behavior of MZMs can be effectively regulated by precisely controlling the magnitude and direction of the magnetic field as well as the parameters of the junction.

6. Conclusions

In the current research, the Josephson junction is a core component in the field of superconducting electronics. To modify the Josephson junction, we propose to insert a middle superconductor strip into a junction. The middle superconducting layer will divide the original continuous 2DEG region into two smaller regions. This modification changes the structure of the electron gas, reducing the quasiparticle trajectory in the 2DEG. Due to the existence of the inserted superconductor, the superconducting proximity effect is enhanced, which could avoid the appearance of soft gaps and provide a possibility for creating stable Majorana zero-energy modes.

Based on the Bogoliubov–de Gennes Hamiltonian on the two-dimensional electron gas and s-wave superconductor regions, we can discretize this continuous Hamiltonian to the tight-binding Hamiltonian in the lattice system. By numerical simulations, we investigate the effect of middle superconductor strips with different widths W and in-plane magnetic

fields B_x on the band structures of Josephson junctions. In the case of no superconductor strips inserted, there is a soft gap in the band structures of the system, and the topological gap disappears when the in-plane magnetic field is zero. The insertion of the middle superconductor strips significantly increases the topological gap of the Josephson junctions, which is of great importance for improving the stability of MZMs. In addition, we also compare the band structures of the modified system with different in-plane magnetic fields B_x. The results show that the modified system can maintain a certain topological gap even at higher in-plane magnetic fields, which demonstrates the robustness of our modified setup in a strong magnetic field environment.

This modified Josephson junction can reduce the destruction of the MZMs by the magnetic field. On the one hand, the introduction of the superconducting phase difference can reduce the critical magnetic field B_{crit} for the topological phase transition of the system. On the other hand, the inserted middle superconductor strips make the topological gap of the system significantly increase, and a more stable MZMs can be maintained even at a strong magnetic field. This modification on the structure of the Josephson junction is more convenient to experiment with, which facilitates future experimental studies and applications. The influence of the superconducting phase difference and the superconducting coupling strength between three s-wave superconductors of the system deserves to be studied in depth. These studies will help us understand the physical properties of modified Josephson junctions more comprehensively, and provide theoretical support for future application development.

Author Contributions: Conceptualization, L.L.; software, Q.W.; writing—original draft preparation, Y.H.; writing—review and editing, Y.H., Z.W. and L.L.; supervision, Z.W. All authors have read and agreed to the published version of the manuscript.

Funding: This work was funded by NSFC Grant Nos. 12147207.

Data Availability Statement: Data are contained within the article.

Acknowledgments: We are grateful to Jun Tao for the useful discussions. This work is supported by NSFC Grant Nos. 12147207. This work is finished on the server from Kun-Lun in Center for Theoretical Physics, School of Physics, Sichuan University.

Conflicts of Interest: The authors declare no conflicts of interest.

References

1. Kitaev, A.Y. Unpaired Majorana fermions in quantum wires. *Physics-Uspekhi* **2001**, *44*, 131–136. [CrossRef]
2. Alicea, J. New directions in the pursuit of Majorana fermions in solid state systems. *Rep. Prog. Phys.* **2012**, *75*, 076501. [CrossRef] [PubMed]
3. Yang, Y.; Yang, B.; Ma, G.; Li, J.; Zhang, S.; Chan, C.T. Non-Abelian physics in light and sound. *Science* **2024**, *383*, eadf9621. [CrossRef] [PubMed]
4. Elliott, S.R.; Franz, M. Colloquium: Majorana fermions in nuclear, particle, and solid-state physics. *Rev. Mod. Phys.* **2015**, *87*, 137–163. [CrossRef]
5. Lutchyn, R.M.; Bakkers, E.P.A.M.; Kouwenhoven, L.P.; Krogstrup, P.; Marcus, C.M.; Oreg, Y. Majorana zero modes in superconductor—Semiconductor heterostructures. *Nat. Rev. Mater.* **2018**, *3*, 52–68. [CrossRef]
6. Jäck, B.; Xie, Y.; Yazdani, A. Detecting and distinguishing Majorana zero modes with the scanning tunnelling microscope. *Nat. Rev. Phys.* **2021**, *3*, 541–554. [CrossRef]
7. Flensberg, K.; von Oppen, F.; Stern, A. Engineered platforms for topological superconductivity and Majorana zero modes. *Nat. Rev. Mater.* **2021**, *6*, 944–958. [CrossRef]
8. Oreg, Y.; Refael, G.; von Oppen, F. Helical Liquids and Majorana Bound States in Quantum Wires. *Phys. Rev. Lett.* **2010**, *105*, 177002. [CrossRef] [PubMed]
9. Aasen, D.; Hell, M.; Mishmash, R.V.; Higginbotham, A.; Danon, J.; Leijnse, M.; Jespersen, T.S.; Folk, J.A.; Marcus, C.M.; Flensberg, K.; et al. Milestones Toward Majorana-Based Quantum Computing. *Phys. Rev. X* **2016**, *6*, 031016. [CrossRef]
10. Yazdani, A.; von Oppen, F.; Halperin, B.I.; Yacoby, A. Hunting for Majoranas. *Science* **2023**, *380*, eade0850. [CrossRef]
11. Leijnse, M.; Flensberg, K. Introduction to topological superconductivity and Majorana fermions. *Semicond. Sci. Technol.* **2012**, *27*, 124003. [CrossRef]
12. Frolov, S.M.; Manfra, M.J.; Sau, J.D. Topological superconductivity in hybrid devices. *Nat. Phys.* **2020**, *16*, 718–724. [CrossRef]

13. Aghaee, M.; Akkala, A.; Alam, Z.; Ali, R.; Alcaraz Ramirez, A.; Andrzejczuk, M.; Antipov, A.E.; Aseev, P.; Astafev, M.; Bauer, B.; et al. InAs-Al hybrid devices passing the topological gap protocol. *Phys. Rev. B* **2023**, *107*, 245423. [CrossRef]
14. Cao, Z.; Chen, S.; Zhang, G.; Liu, D.E. Recent progress on Majorana in semiconductor-superconductor heterostructures—Engineering and detection. *Sci. China Phys. Mech. Astron.* **2023**, *66*, 267003. [CrossRef]
15. Marra, P. Majorana nanowires for topological quantum computation. *J. Appl. Phys.* **2022**, *132*, 231101. [CrossRef]
16. Fu, L.; Kane, C.L. Superconducting Proximity Effect and Majorana Fermions at the Surface of a Topological Insulator. *Phys. Rev. Lett.* **2008**, *100*, 096407. [CrossRef] [PubMed]
17. Lutchyn, R.M.; Sau, J.D.; Das Sarma, S. Majorana Fermions and a Topological Phase Transition in Semiconductor-Superconductor Heterostructures. *Phys. Rev. Lett.* **2010**, *105*, 077001. [CrossRef]
18. Sau, J.D.; Lutchyn, R.M.; Tewari, S.; Das Sarma, S. Generic New Platform for Topological Quantum Computation Using Semiconductor Heterostructures. *Phys. Rev. Lett.* **2010**, *104*, 040502. [CrossRef] [PubMed]
19. Li, Y.; Chan, Y.h.; Hlevyack, J.A.; Bowers, J.W.; Chou, M.Y.; Chiang, T.C. Topological Quantum Well States in Pb/Sb Thin-Film Heterostructures. *ACS Nano* **2024**, *18*, 10243–10248. [CrossRef]
20. Pientka, F.; Keselman, A.; Berg, E.; Yacoby, A.; Stern, A.; Halperin, B.I. Topological Superconductivity in a Planar Josephson Junction. *Phys. Rev. X* **2017**, *7*, 021032. [CrossRef]
21. Hell, M.; Leijnse, M.; Flensberg, K. Two-Dimensional Platform for Networks of Majorana Bound States. *Phys. Rev. Lett.* **2017**, *118*, 107701. [CrossRef] [PubMed]
22. Kim, M.D. Circulator function in a Josephson junction circuit and braiding of Majorana zero modes. *Sci. Rep.* **2021**, *11*, 1826. [CrossRef] [PubMed]
23. Yuan, T.; Zhou, F.; Chen, S.; Xiang, S.; Song, K.; Zhao, Y. Multipurpose Quantum Simulator Based on a Hybrid Solid-State Quantum Device. *Symmetry* **2019**, *11*, 467. [CrossRef]
24. Ren, H.; Pientka, F.; Hart, S.; Pierce, A.T.; Kosowsky, M.; Lunczer, L.; Schlereth, R.; Scharf, B.; Hankiewicz, E.M.; Molenkamp, L.W.; et al. Topological superconductivity in a phase-controlled Josephson junction. *Nature* **2019**, *569*, 93–98. [CrossRef] [PubMed]
25. Paudel, P.P.; Smith, N.O.; Stanescu, T.D. Disorder effects in planar semiconductor-superconductor structures: Majorana wires versus Josephson junctions. *arXiv* **2024**, arXiv:2405.12192.
26. Pan, X.H.; Chen, L.; Liu, D.E.; Zhang, F.C.; Liu, X. Majorana Zero Modes Induced by the Meissner Effect at Small Magnetic Field. *Phys. Rev. Lett.* **2024**, *132*, 036602. [CrossRef] [PubMed]
27. Lesser, O.; Oreg, Y. Majorana zero modes induced by superconducting phase bias. *J. Phys. D Appl. Phys.* **2022**, *55*, 164001. [CrossRef]
28. Fornieri, A.; Whiticar, A.M.; Setiawan, F.; Portolés, E.; Drachmann, A.C.C.; Keselman, A.; Gronin, S.; Thomas, C.; Wang, T.; Kallaher, R.; et al. Evidence of topological superconductivity in planar Josephson junctions. *Nature* **2019**, *569*, 89–92. [CrossRef] [PubMed]
29. Flensberg, K. Tunneling characteristics of a chain of Majorana bound states. *Phys. Rev. B* **2010**, *82*, 180516. [CrossRef]
30. Valentini, M.; Peñaranda, F.; Hofmann, A.; Brauns, M.; Hauschild, R.; Krogstrup, P.; San-Jose, P.; Prada, E.; Aguado, R.; Katsaros, G. Nontopological zero-bias peaks in full-shell nanowires induced by flux-tunable Andreev states. *Science* **2021**, *373*, 82–88. [CrossRef]
31. Dartiailh, M.C.; Mayer, W.; Yuan, J.; Wickramasinghe, K.S.; Matos-Abiague, A.; Žutić, I.; Shabani, J. Phase Signature of Topological Transition in Josephson Junctions. *Phys. Rev. Lett.* **2021**, *126*, 036802. [CrossRef] [PubMed]
32. Jeon, S.; Xie, Y.; Li, J.; Wang, Z.; Bernevig, B.A.; Yazdani, A. Distinguishing a Majorana zero mode using spin-resolved measurements. *Science* **2017**, *358*, 772–776. [CrossRef]
33. Sun, L.; DiCarlo, L.; Reed, M.D.; Catelani, G.; Bishop, L.S.; Schuster, D.I.; Johnson, B.R.; Yang, G.A.; Frunzio, L.; Glazman, L.; et al. Measurements of Quasiparticle Tunneling Dynamics in a Band-Gap-Engineered Transmon Qubit. *Phys. Rev. Lett.* **2012**, *108*, 230509. [CrossRef]
34. Laeven, T.; Nijholt, B.; Wimmer, M.; Akhmerov, A.R. Enhanced Proximity Effect in Zigzag-Shaped Majorana Josephson Junctions. *Phys. Rev. Lett.* **2020**, *125*, 086802. [CrossRef] [PubMed]
35. Takei, S.; Fregoso, B.M.; Hui, H.Y.; Lobos, A.M.; Das Sarma, S. Soft Superconducting Gap in Semiconductor Majorana Nanowires. *Phys. Rev. Lett.* **2013**, *110*, 186803. [CrossRef]
36. Heiss, W. *Quantum Dots: A Doorway to Nanoscale Physics*; Springer: Berlin/Heidelberg, Germany, 2005.
37. Haim, A.; Stern, A. Benefits of Weak Disorder in One-Dimensional Topological Superconductors. *Phys. Rev. Lett.* **2019**, *122*, 126801. [CrossRef]
38. Hassan, S.A.; Wu, B.H.; Xu, X.F.; Wang, C.R.; Cao, J.C. Bending effect on the Majorana bound states in planar Josephson junctions. *J. Phys. Condens. Matter* **2021**, *33*, 385001. [CrossRef]
39. van Heck, B.; Mi, S.; Akhmerov, A.R. Single fermion manipulation via superconducting phase differences in multiterminal Josephson junctions. *Phys. Rev. B* **2014**, *90*, 155450. [CrossRef]
40. Bardarson, J.H. A proof of the Kramers degeneracy of transmission eigenvalues from antisymmetry of the scattering matrix. *J. Phys. A Math. Theor.* **2008**, *41*, 405203. [CrossRef]
41. Beenakker, C.W.J. Universal limit of critical-current fluctuations in mesoscopic Josephson junctions. *Phys. Rev. Lett.* **1991**, *67*, 3836–3839. [CrossRef]

42. Oliinyk, A.; Yatsuta, I.; Malomed, B.; Yakimenko, A. Symmetry Breaking in Interacting Ring-Shaped Superflows of Bose–Einstein Condensates. *Symmetry* **2019**, *11*, 1312. [CrossRef]
43. Akramov, M.; Askerzade, I.; Salati, M.; Karpova, O. Bogoliubov-de Gennes equation on graphs: A model for tree-branched Majorana wire network. In *Proceedings of the Journal of Physics: Conference Series*; IOP Publishing: Bristol, UK, 2023; Volume 2667, p. 012032.
44. Pekerten, B.; Pakizer, J.D.; Hawn, B.; Matos-Abiague, A. Anisotropic topological superconductivity in Josephson junctions. *Phys. Rev. B* **2022**, *105*, 054504. [CrossRef]
45. Sakurai, J.J.; Napolitano, J. *Modern Quantum Mechanics*; Cambridge University Press: Cambridge, UK, 2020. [CrossRef]
46. Altland, A.; Zirnbauer, M. Nonstandard symmetry classes in mesoscopic normal-superconducting hybrid structures. *Phys. Rev. B* **1997**, *55*, 1142–1161. [CrossRef]
47. Ryu, S.; Schnyder, A.P.; Furusaki, A.; Ludwig, A.W.W. Topological insulators and superconductors: Tenfold way and dimensional hierarchy. *New J. Phys.* **2010**, *12*, 065010. [CrossRef]
48. Melo, A.; Rubbert, S.; Akhmerov, A.R. Supercurrent-induced Majorana bound states in a planar geometry. *SciPost Phys.* **2019**, *7*, 039. [CrossRef]
49. Groth, C.W.; Wimmer, M.; Akhmerov, A.R.; Waintal, X. Kwant: A software package for quantum transport. *New J. Phys.* **2014**, *16*, 063065. [CrossRef]
50. Huang, Y.; Wang, Q.; Li, L.; Wen, Z. Stable Majorana zero-energy modes in two-dimensional Josephson Junctions. *Zenodo* **2024**. [CrossRef]
51. Kuiri, D.; Nowak, M.P. Non-local transport signatures of topological superconductivity in a phase-biased planar Josephson junction. *Phys. Rev. B* **2023**, *108*, 205405. [CrossRef]